Journal of X-Ray Science and Technology 13 (2005) 9–21
IOS Press

A practical software platform of integrated reconstruction algorithms and forward algorithms for 2D industrial CT

Hui Li[a], Zhaotian Zhang[b] and Jie Tian[a,*]
[a]*Medical Image Processing Group, Key Laboratory of Complex Systems and Intelligence Science, Institute of Automation, Chinese Academy of Sciences, P.O.Box 2728, Beijing 100080, China*
[b]*Department of Information Science, National Natural Science Foundation of China, Beijing 100085, China*

Received 10 September 2004
Revised 10 October 2004
Accepted 28 October 2004

Abstract. Computed tomography plays an important role in industrial non-destructive testing, medical applications, astronomy and many other fields to analyze inner structures of scanned objects. This article addresses a new development of non-destructive testing software platform to efficiently detect inner flaws of space industrial components. As the key of our software, reconstruction algorithms of 2D industrial computed tomography including preprocess of raw data, re-arrange algorithm and filtered back-projection algorithms have been described in detail in this article. Experimental results with four groups of real raw data from China Aerospace Science and Technology Corporation confirmed the accuracy of the reconstruction algorithm in our software. Forward algorithm of 2D industrial computed tomography is another important component of our software, which conveniently generates parallel-beam and fan-beam raw data with given parameters.

Keywords: Reconstruction algorithms, forward algorithms, industrial CT, imaging data preprocess

1. Introduction

Computed tomography (CT) has been widely used in many fields such as industrial non-destructive testing and medical diagnosis [1], because the inner structures especially flaws of various devices can be non-invasively detected. A practical software platform was developed for the reconstruction of two-dimensional (2D) tomographic images from raw data of industrial CT. Our software is focused on parallel-beam CT and fan-beam CT as those have been pervasively used in China.

Forward algorithm and inverse reconstruction algorithm of 2D industrial CT are two key points in this article. According to the propagation theory of X-rays, forward algorithms can generate various simulated data of parallel-beam and fan-beam. Moreover, the investigation of forward algorithms can help debug and verify inverse reconstruction algorithms.

*Corresponding author. Tel.: +86 10 625 32105; Fax: +86 10 625 27995; E-mail: tian@doctor.com.

Besides forward algorithm of CT, reconstruction algorithm is apparently the key of our non-destructive software. There are different reconstruction algorithms according to different scanning and detecting models of CT [2–13]. It is well known that filtered back-projection (FBP) algorithm is efficiently used in parallel-beam reconstruction and fan-beam reconstruction [2–7]. Though fan-beam filtered back-projection (FFBP) algorithms are also used for images reconstruction directly from fan-beam data, the spatially variant weighting factor in FFBP algorithm can significantly amplify data noise and aliasing artifacts in the situations where focal lengths are comparable to or smaller than the size of the field of measurement (FOM) [2–8]. As an alternative, we generate parallel-beam data by interpolating fan-beam data and then reconstruct images with the computationally efficient and numerically stable parallel-beam FBP.

Because mechanic devices of CT usually cause some inevitable errors, raw data must be preprocessed and corrected to ensure the precision of reconstruction algorithms. In this article, we propose a convenient algorithm to efficiently eliminate these mechanic errors through directly analyzing and rectifying raw data.

In the following sections, we describe the forward theory of CT (Section 2), introduce preprocess algorithm of raw data (Section 3), present FBP reconstruction algorithms of 2D industrial CT (Section 4), show experimental results of our non-destructive software (Section 5), and present our conclusion (Section 6).

2. Principles of forward algorithms in CT

To study forward algorithm and reconstruction algorithm of 2D industrial CT, four indispensable parameters must be given, including the rotation samples Ns of the X-ray source along its circular trajectory, the total number Np of X-ray projections in each beam, the distance D between the X-ray source and its rotating center, and the incident intensity I_0 of the X-ray beams. The scanned area is assumed as a circle with the radius R and the centre O for brevity. And the X-ray source anticlockwise rotates along a circular orbit with the centre O.

Forward algorithms simulate the attenuation of X-rays from non-diffracting sources as they propagate in a straight line through the scanned object. Assume the object whose attenuation coefficient with respect to X-rays at the point (x, y) is $f(x, y)$. The total attenuation of X-ray beam L can be represented by a line integral [2]:

$$P_\theta(t) = \int_L f(x,y)ds = \int_{-\infty}^{+\infty}\int_{-\infty}^{+\infty} f(x,y)\delta(x\cos\theta + y\sin\theta - t)dxdy \tag{1}$$

where $\begin{matrix} t = x\cos\theta + y\sin\theta \\ s = -x\sin\theta + y\cos\theta \end{matrix}$. The intensity of L past the object is calculated by

$$I = I_0 e^{-\int_L f(x,y)ds}. \tag{2}$$

2.1. Forward algorithm of parallel-beam

As shown in Fig. 1, the integral parallel-beam raw data are made up of the attenuated intensity values of Ns beams (e.g. *PB1*, *PBm*), each of which contains Np X-ray projections. Take an example, we choose the projection $n(1 \leqslant n \leqslant Np)$ (e.g. $n = 2$) of the *PBm* parallel-beam (i.e. *PBm-n*) to calculate

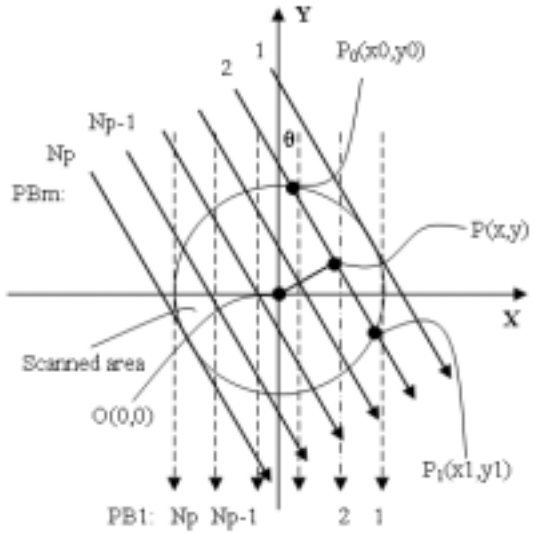

Fig. 1. Schematic of forward algorithm used in 2D parallel-beam CT. PB1 and PBm are parallel-beams containing Np parallel X-ray projections. θ is the rotation angle between PB1 and PBm. P_0 and P_1 are two interactions of projection PBm-2 and the circular scanned area whose center is point O. Line OP is perpendicular to line P_0P_1.

its attenuated intensity. Points P_0 and P_1 are two intersections of projection *PBm-n* and the circular scanned area. The coordinates of P_0 and P_1 are calculated as follows:

$$\begin{aligned} x_0 &= \left|\overrightarrow{OP}\right|\cos\theta - \left|\overrightarrow{P_0P}\right|\sin\theta, \quad y_0 = \left|\overrightarrow{OP}\right|\sin\theta + \left|\overrightarrow{P_0P}\right|\cos\theta \\ x_1 &= \left|\overrightarrow{OP}\right|\cos\theta + \left|\overrightarrow{P_0P}\right|\sin\theta, \quad y_1 = \left|\overrightarrow{OP}\right|\sin\theta - \left|\overrightarrow{P_0P}\right|\cos\theta, \\ \left|\overrightarrow{OP}\right| &= R-(n-1)\Delta d, \qquad \left|\overrightarrow{P_0P}\right| = (R^2 - \left|\overrightarrow{OP}\right|^2)^{\frac{1}{2}} \end{aligned} \tag{3}$$

where θ is the rotation angle between *PB1* and *PBm*, $\Delta d = \frac{2R}{Np-1}$ is the interval of two adjacent parallel-beam projections, and $\overrightarrow{OP}\perp\overrightarrow{P_0P_1}$. According to Eqs (1) and (2), the attenuated intensity of the projection *PBm-n* is computed by:

$$p(m,n) = I_0 \bullet e^{-\int_{P_0P_1}\mu(s)ds}, \tag{4}$$

where $\mu(s)$ is the attenuation coefficient function along the line $\overrightarrow{P_0P_1}$, and the 2D matrix $p(m,n)$ is the raw data matrix involving the attenuation values of all X-ray projections propagating through the scanned area.

2.2. Forward algorithm of fan-beam

Besides parameters Ns, Np, D and I_0, the fan angle Af is another indispensable parameter in 2D fan-beam CT. As shown in Fig. 2, the integral fan-beam raw data are made up of the attenuated intensity values of Ns fan-beams (e.g. *FB1*, *FBm*), each of which has Np X-ray projections.

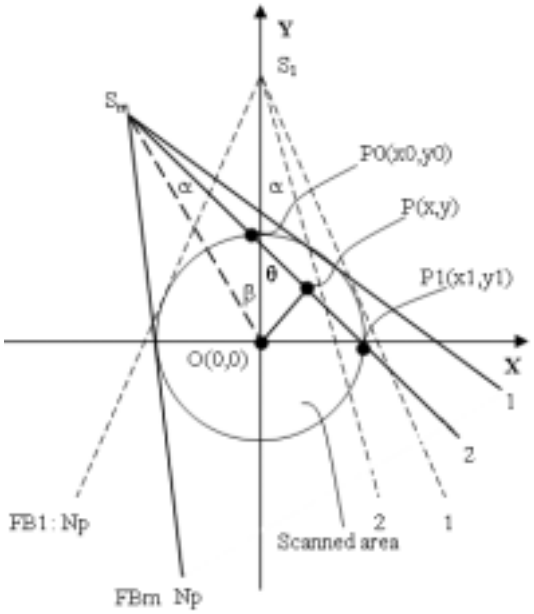

Fig. 2. Schematic of forward algorithm used in fan-beam CT. FB1 and FBm are fan-beams containing Np fan X-ray projections. α is the angle between $\overrightarrow{OS_m}$ and projection FBm-2. β is the rotation angle between FB1 and FBm (i.e. the angle between $\overrightarrow{OS_1}$ and $\overrightarrow{OS_m}$). θ is angle between projection FBm-2 and Y-axis. P_0 and P_1 are two interactions of projection FBm-2 and the circular scanned area whose center is point O. Line OP is perpendicular to line P_0P_1.

We optionally choose the projection $n(1 \leqslant n \leqslant Np)$ of the *FBm* fan-beam (i.e. *FBm-n*), then calculate the attenuated intensity after it passing the scanned area. Points P_0 and P_1 are two intersections of projection *FBm-n* and the circular scanned area. When vector $\overrightarrow{OP}$ satisfies $\overrightarrow{OP} \perp \overrightarrow{P_0P_1}$, $\left|\overrightarrow{OP}\right|$ and $\left|\overrightarrow{P_0P}\right|$ are computed by

$$\left|\overrightarrow{OP}\right| = D\sin\alpha, \quad \left|\overrightarrow{P_0P}\right| = (R^2 - \left|\overrightarrow{OP}\right|^2)^{\frac{1}{2}}, \tag{5}$$

where $\alpha = Af/2 - (n-1)\Delta\alpha$ and $\Delta\alpha$ is the angle between two adjacent fan-beam projections. Then, the coordinates of points P_0 and P_1 can be calculated as follows:

$$\begin{aligned} x_0 &= \left|\overrightarrow{OP}\right|\cos\theta - \left|\overrightarrow{P_0P}\right|\sin\theta, \quad y_0 = \left|\overrightarrow{OP}\right|\sin\theta + \left|\overrightarrow{P_0P}\right|\cos\theta \\ x_1 &= \left|\overrightarrow{OP}\right|\cos\theta + \left|\overrightarrow{P_0P}\right|\sin\theta, \quad y_1 = \left|\overrightarrow{OP}\right|\sin\theta - \left|\overrightarrow{P_0P}\right|\cos\theta \end{aligned}, \tag{6}$$

where $\theta = \alpha + \beta$ and β is the rotation angle between *FB1* and*FBm* (i.e. the angle between vector $\overrightarrow{OS_1}$ and $\overrightarrow{OS_m}$). The attenuated intensity of the projection *FBm-n* as well as the raw data matrix $p(m,n)$ can also be obtained by Eq. (5).

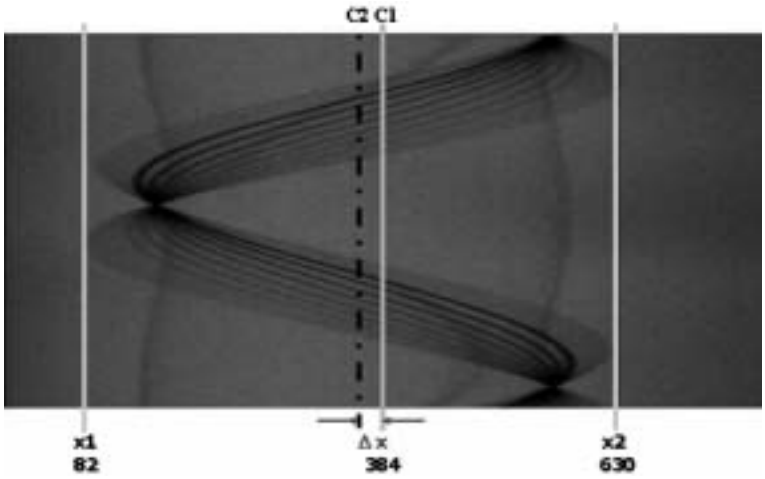

Fig. 3. Original raw data image. C1 is the center line of the whole original raw data image. C2, x1 and x2 are the center line, the left boundary line and the right boundary line of the image area including the meaningful information respectively. Δx is the offset between line C1 and C2.

3. Preprocess of raw data in 2D industrial CT

Preprocess must be performed prior to the reconstruction operation, since mechanical devices of CT usually have unavoidable impacts on raw data during scanning and detecting. In our experiences, a common problem caused by mechanical devices of CT is that the rotation center of the source-detector is not in center of the scanned area, which usually results in poor reconstruction quality. Hence, the raw data image isn't bilaterally symmetric. In general, the central line (e.g. $C1$shown in Fig. 3) of the whole raw data image represents the rotation center of the source-detector. After the background is removed, the central line (e.g. $C2$ shown in Fig. 3) of the image area including meaningful information represents the center of the scanned area. The offset of these two centers (i.e. the interval between line $C1$ and $C2$ in Fig. 3) is generally adjusted according to operators' experience, which may lead to inaccuracy and discommodiousness in practice. We proposed an algorithm to automatically search for the optimal offset Δx according to original raw data as follows.

First, raw data are inputted into a matrix $M(i,j) \quad 1 \leqslant i \leqslant Ns,\ 1 \leqslant j \leqslant Np$, where parameters i and j respectively represents the rotation index of the X-ray beam and the index of the X-ray projection. Then, the maximum matrix $Max(j)$, constituted by all the maximum in each column of $M(i,j)$, is obtained. According to prior knowledge, the grey-level threshold T_B of the background is directly obtained from original raw data. Hence, the offset is calculated by

$$\begin{array}{l} \Delta W = Np - I_{\max} - I_{\min} \\ \Delta x = \Delta W/2 \end{array}, \tag{7}$$

where $I_{\min}$ and $I_{\max}$ are the minimum and maximum of projection indices satisfying the condition $Max(j) > T_B$. After ΔW columns are deleted from the original raw data matrix $M(i,j)$, the two lines $C1$ and $C2$ are superposed. Then the modified raw data matrix is ready to be reconstructed.

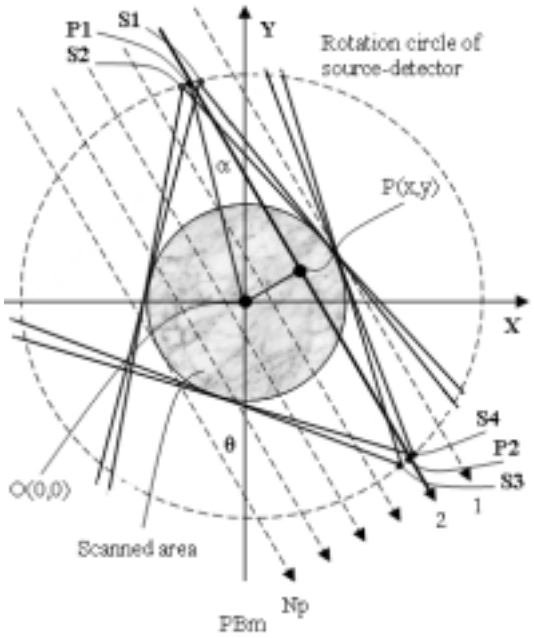

Fig. 4. Schematic of re-arranging fan projections. PB1 and PBm are parallel-beams containing Np parallel X-ray projections. P_1 and P_2 are two interactions of projection PBm-2 and the circular scanned area whose center is point O. S1 and S2 are two fan-beam source positions closest to P_1. S3 and S4 are two fan-beam source positions closest to P_2. Line OP is perpendicular to line P_0P_1. α is the angle between $\overrightarrow{OP_1}$ and parallel projection PBm-2. θ is angle between parallel-beam PBm and Y-axis.

4. Filtered back-projection algorithms of 2D industrial CT

In China, filtered back-projection (FBP) algorithm is popular and currently used in almost all applications of industrial CT. Derived from the Fourier Slice Theorem [2–4] by rewriting the inverse Fourier transform in polar coordinates, FBP algorithm has been shown to be extremely accurate and amenable to fast implementation [5–9].

4.1. Filtered back-projection algorithm for parallel projections

The Fourier Slice Theorem states that 1D Fourier transform $S_\theta(w)$ of a parallel projection of an image $f(x,y)$ taken at angle θ gives a slice of the 2D transform $F(u,v)$, subtending an angle θ with the u-axis. Therefore, the object function $f(x,y)$ can then be recovered by using 2D inverse Fourier transform.

$$f(x,y) = \int_{-\infty}^{+\infty}\int_{-\infty}^{+\infty} F(u,v)e^{j2\pi(ux+vy)}dudv. \tag{8}$$

With the coordinate transformation $\begin{matrix} u = w\cos\theta \\ v = w\sin\theta \end{matrix}$, Eq. (8) can be written as its polar function

$$f(x,y) = \int_0^{2\pi}\int_0^{+\infty} F(w,\theta)e^{j2\pi w(x\cos\theta+y\sin\theta)}wdwd\theta. \tag{9}$$

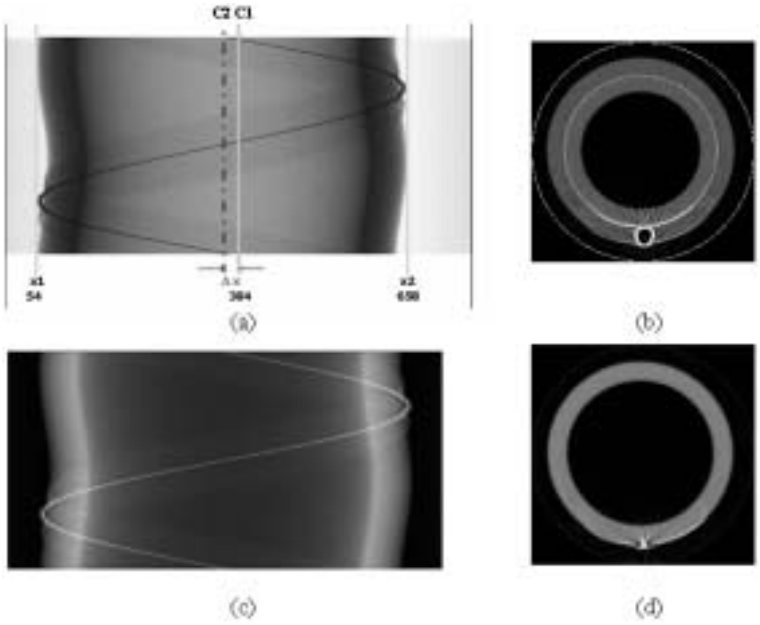

Fig. 5. Raw data image and reconstructed image of the fan-beam raw data from CASC. The 3D scanned object resembles a barrel with a small high-density object embedded on the outer surface. (a) Original raw data image, image size (pixels): 358×768. (b) Reconstructed image using the reconstruction algorithm without preprocess of raw data. (c) Re-arranged image after preprocess. (d) Reconstructed image using reconstruction algorithm with the re-arranged raw data. C1 is the center line of the whole original raw data image. C2, x1 and x2 are the center line, the left boundary line and the right boundary line of the image area including the meaningful information respectively. Δx is the offset between line C1 and C2.

According to the Fourier Slice Theorem, Eq. (9) can also be expressed as

$$\begin{array}{l} f(x,y) = \int_0^{\pi} \int_{-\infty}^{+\infty} S_\theta(w) e^{j2\pi wt} \, |w| dw d\theta = \int_0^{\pi} Q_\theta(t) d\theta \\ t = x\cos\theta + y\sin\theta \end{array}, \tag{10}$$

where $Q_\theta(x\cos\theta + y\sin\theta) = Q_\theta(t) = \int_{-\infty}^{+\infty} S_\theta(w) \, |w| \, e^{j2\pi wt} dw$.

4.2. Filtered back-projection algorithms for fan projections

There are two types of fan projections depending on whether the projection is sampled at equiangular intervals or equispaced intervals. Fan-beam filtered back-projection (FFBP) algorithms are used to directly reconstruct images from these two types of projections [5–7]. However, the spatially variant weighting factor in the FFBP algorithm not only increases the computational load, but also significantly amplifies data noise and aliasing artifacts when the focal lengths are comparable to or smaller than the size of FOM [8]. As an alternative, we re-arrange the fan-beam data to parallel-beam data and reconstruct images by using the computationally efficient and numerically stable FBP.

The principal aim of our re-arrange algorithm is to search eight projections from given fan-beam raw data, which are closest to the parallel projection to be calculated. Then, each parallel projection can be easily obtained by bilinear interpolation method. Except for θ and α, other parameters of parallel-beams and fan-beams are defined as Section 2. As shown in Fig. 4, projection $n(1 \leqslant n \leqslant Np)$ of the *PBm* parallel-beam (*PBm-n*) is an arbitrary parallel-beam projection whose detected value is unknown. There

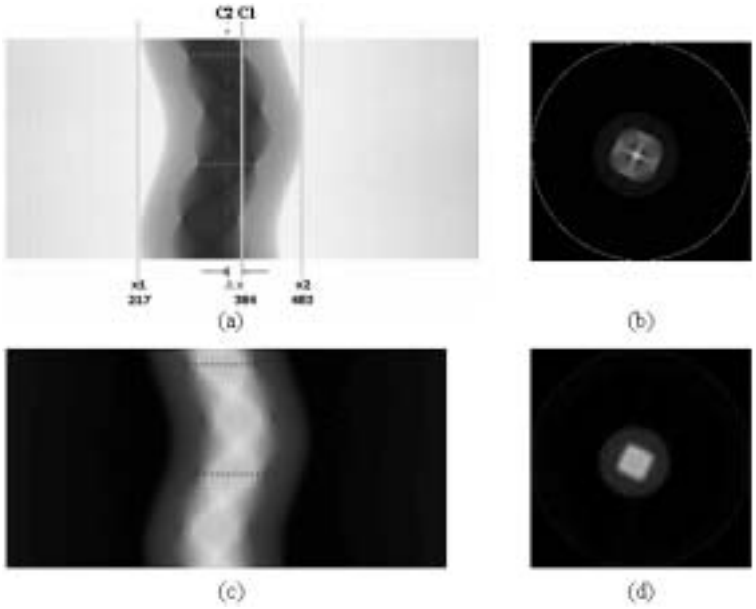

Fig. 6. Raw data image and reconstructed image of the fan-beam raw data from CASC. The cross section of the 3D scanned object involves regular concaves and convexes. (a) Original raw data image, image size (pixels): 358×768. (b) Reconstructed image using the reconstruction algorithm without preprocess of raw data. (c) Re-arranged image after preprocess. (d) Reconstructed image using reconstruction algorithm with the re-arranged raw data. C1 is the center line of the whole original raw data image. C2, x1 and x2 are the center line, the left boundary line and the right boundary line of the image area including the meaningful information respectively. Δx is the offset between line C1 and C2.

are two intersections $P1$ and $P2$ between the projection *PBm-n* and the rotation circle of the source-detector in Fig. 4. According to $P1$ and $P2$, four positions, $S1$, $S2$, $S3$, and $S4$, of the X-ray source can be obtained, which contain the fan-beam projections closest to the parallel-beam projection *PBm-n*. The indices of $S1$, $S2$, $S3$ and $S4$ are $m1$, $m2$, $m3$ and $m4$ computed by

$$\begin{aligned} m1 &= Int(ANG(\theta - \alpha)/\Delta\beta) \\ m2 &= m1 + 1 \\ m3 &= Int(ANG(\pi + \theta + \alpha)/\Delta\beta)\text{'} \\ m4 &= m3 + 1 \end{aligned} \tag{11}$$

$$\text{where} \quad \begin{cases} \alpha = \tan^{-1}(\left|\overrightarrow{OP}\right| / \left|\overrightarrow{PP_1}\right|) \\ \left|\overrightarrow{OP}\right| = R - (n-1)\Delta d \\ \left|\overrightarrow{PP_1}\right| = (D^2 - \left|\overrightarrow{OP}\right|^2)^{\frac{1}{2}} \end{cases}, \tag{12}$$

$ANG(x) = \begin{cases} x & 0 \leqslant x \leqslant 2\pi \\ x - 2\pi & x > 2\pi \\ x + 2\pi & x < 0 \end{cases}$, $Int(x)$ returns the largest integer that is less than or equal to x, θ is the angle between parallel-beam *PBm* and the Y-axis, and $\Delta\beta$ is the angle between the two adjacent fan-beams.

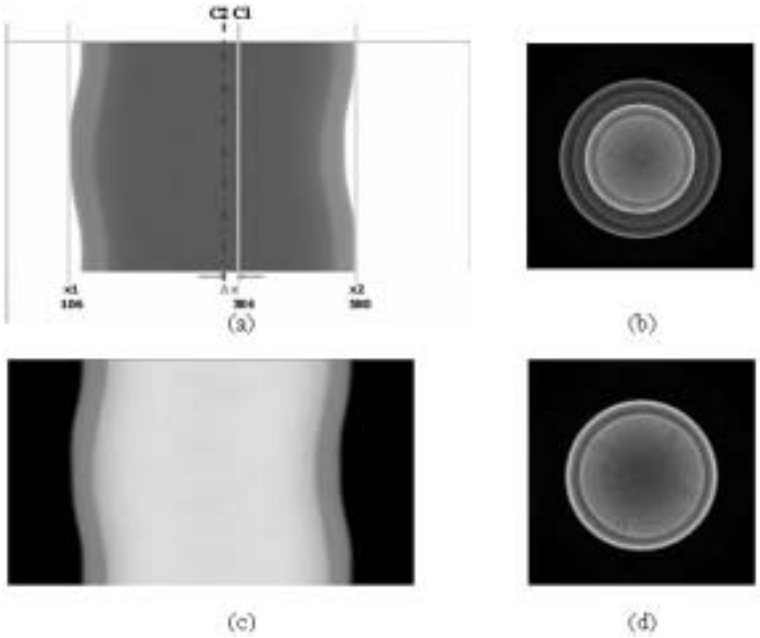

Fig. 7. Raw data image and reconstructed image of the fan-beam raw data from CASC. The cross section of the 3D scanned object is a circular area with regular subtle structures. (a) Original raw data image, image size (pixels): 384×768. (b) Reconstructed image using the reconstruction algorithm without preprocess of raw data. (c) Re-arranged image after preprocess. (d) Reconstructed image using reconstruction algorithm with the re-arranged raw data. C1 is the center line of the whole original raw data image. C2, x1 and x2 are the center line, the left boundary line and the right boundary line of the image area including the meaningful information respectively. Δx is the offset between line C1 and C2.

Each of the four fan-beams, *FBm1*, *FBm2*, *FBm3* and *FBm4*, has two projections closest to the parallel-beam projection *PBm-n*. The indices of the two projections, $n1$ and $n2$, are calculated as:

$$\begin{array}{l} n1 = Int(\alpha/\Delta\alpha) \\ n2 = n1 + 1 \end{array}, \tag{13}$$

where $\Delta\alpha$ is the angle between the two adjacent projections of one fan-beam. The detected value of parallel-beam projection *PBm-n* is calculated by bilinear interpolation:

$$\begin{array}{l} \mathrm{temp1} = (Rn1 * f(m1, n1) + Pn1 * f(m1, n2) + Rn1 * f(m3, n1) + Pn1 * f(m3, n2))/2 \\ \mathrm{tmep2} = (Rn1 * f(m2, n1) + Pn1 * f(m2, n2) + Rn1 * f(m4, n1) + Pn1 * f(m4, n2))/2 \\ p(m, n) = (Rm1 * temp1 + Pm1 * \mathrm{temp2} + Rm3 * \mathrm{temp1} + Pm3 * \mathrm{temp2})/2 \end{array}, \tag{14}$$

$$Pn1 = n1 - Int(n1), \quad Rn1 = 1 - Pn1$$

where $Pm1 = m1 - Int(m1), \quad Rm1 = 1 - Pm1$, 2D matrixes $p(m, n)$ and $f(m, n)$ are the raw data
$Pm3 = m3 - Int(m3), Rm3 = 1 - Pm3$

matrixes involving the attenuation values of all parallel-beam and fan-beam projections transporting through the scanned area.

After the detection values of all parallel-beam projections are obtained, the tomography image is reconstructed by using the filtered back-projection algorithm for parallel projections.

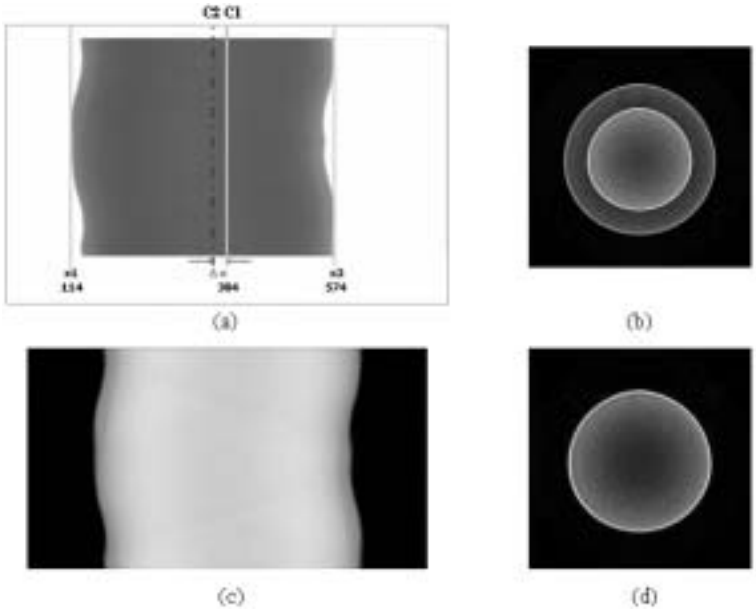

Fig. 8. Raw data image and reconstructed image of the fan-beam raw data from CASC. The cross section of the 3D scanned object resembles a circular area on the whole. (a) Original raw data image, image size (pixels): 384×768. (b) Reconstructed image using the reconstruction algorithm without preprocess of raw data. (c) Re-arranged image after preprocess. (d) Reconstructed image using reconstruction algorithm with the re-arranged raw data. C1 is the center line of the whole original raw data image. C2, x1 and x2 are the center line, the left boundary line and the right boundary line of the image area including the meaningful information respectively. Δx is the offset between line C1 and C2.

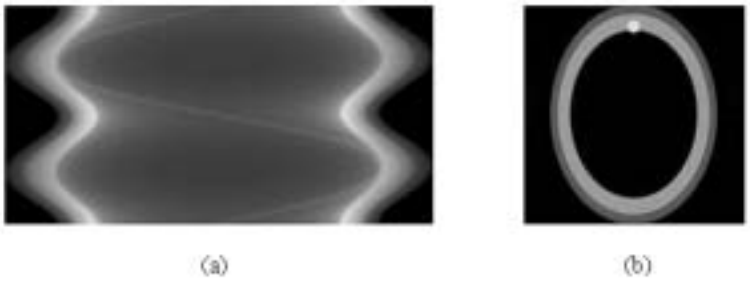

Fig. 9. Simulated raw data image generated by the presented forward algorithm of fan-beam, and the reconstructed image obtained by the presented reconstruction algorithm. (a) Simulated raw data image. Image size (pixels): 360×700; the fan angel is 10 degree; the distance between the X-ray source and its rotation center is 500 millimeter. (b) Reconstructed image of simulated raw data.

5. Experimental results

The accuracy of our non-destructive testing software is verified by conducting five experiments in this section. Fan-beam raw data of Experiment 1, 2, 3, and 4 were obtained from the 703^{th} Institute of China Aerospace Science and Technology Corporation (CASC). And the raw data of Experiment 5 are generated by the forward algorithm of fan-beam presented in this article. Four prerequisite parameters of each experiment are Ns, Np, Af, and D defined in Section 2. As shown in Figs 5, 6, 7 and 8, line $C1$ represents the rotation center of the source-detector. Line $C2$, $x1$, and $x2$ are the center line, the left boundary line and the right boundary line of the image area including the meaningful information

respectively. Parameters $I_{\min}$, $I_{\max}$, and Δx are defined in Section 3.

5.1. Raw data images and reconstructed images

In Experiment 1, the image size of the original raw data is 358×768 pixels, which represents that the rotation samples of the X-ray source is 358 and each fan-beam has 768 projections. The fan angle is 11.2 degree. And the distance between the X-ray source and its rotating center is 700 millimeter. From the original raw data image shown in Fig. 5(a), we can obtain $I_{\min} = 54,\ I_{\max} = 658$. With the four parameters $Ns = 358, Np = 768, Af = 11.2^\circ, D = 700$ mm and Eq. (7), there are 56 columns to be deleted from the original raw data matrix. Then the re-arranged image (Fig. 5(c)) can be obtained from the preprocessed raw data. According to prior knowledge, the 3D scanned object of Experiment 1 resembles a barrel with a small high-density object embedded on the outer surface. The tomographic image (Fig. 5(d)) reconstructed by our presented algorithms efficiently displays the 2D inner structure of the scanned object. However, the reconstructed image (Fig. 5(b)) obtained by the reconstruction algorithm without preprocess of raw data has many artifacts and serious distortions.

Parameters Ns, Np, Af, and D of Experiment 2 are the same as those of Experiment 1. From the original raw data image (Fig. 6(a)) and Eq. (7), we can obtain $I_{\min} = 217,\ I_{\max} = 483, \Delta W = 68$. After 68 columns are deleted from the original raw data matrix, the modified fan-beam raw data is ready to be re-arranged to parallel-beam data shown in Fig. 6(c). Prior knowledge reads that the cross section of the 3D scanned object involves regular concaves and convexes. According to the preprocess algorithm and reconstruction algorithm, the 2D reconstructed image (Fig. 6(d)) correctly shows those regular concaves and convexes of the scanned object. Without preprocess of raw data, the reconstruction algorithm leads to artifacts and distortions shown in Fig. 6(b).

In Experiment 3, the image size of the original raw data (Fig. 7(a)) is 384×768 pixels. The fan angle is 9.7 degree. And the distance between the X-ray source and its rotating center is 10 millimeter. According to the preprocess algorithm and parameters $I_{\min} = 54,\ I_{\max} = 658$, 82 columns of the original raw data matrix need to be deleted. Prior knowledge of Experiment 3 is that the cross section of the 3D scanned object is a circular area with regular subtle structures. As shown in Fig. 7(d), the whole shape of the scanned object and subtle features of the inner structure have been reconstructed by our presented algorithms. However, artifacts and distortions obviously exist in the reconstructed image (Fig. 7(b)) obtained by the traditional reconstruction algorithm without preprocess.

According to the raw data file of Experiment 4, parameters are obtained as $Ns = 384, Np = 768, Af = 9.7^\circ,\ D = 10$ mm,$I_{\min} = 217,\ I_{\max} = 483$. Then, the number of columns to be cut from the original raw data matrix is calculated by $\Delta W = 2\Delta x = Np - I_{\max} - I_{\min} = 80$. Prior knowledge reads that the cross section of the 3D scanned object resembles a circular area on the whole. As shown in Figs 8(b) and (d), the inner structure reconstructed by our presented algorithm is more correct than that reconstructed by algorithms without preprocess.

5.2. Simulated raw data image and reconstructed image

Given the four parameters (i.e. Ns, Np, Af, D) and the attenuation coefficient function $f(x, y)$ of the scanned cross section, many parallel-beam raw data and fan-beam raw data are easily generated by the presented forward algorithms in Section 2. With our software, it is convenient to build a raw-data database for testing various reconstruction algorithms. Take the generation of fan-beam raw data as an

example. The four parameters are set as $Ns = 360, Np = 700, Af = 10^\circ, D = 500$ mm. And the attenuation coefficient function $f(x, y)$ of the scanned object is described as

$$f(x,y) = \begin{cases} 0.4 & \text{if } (x^2/9 + y^2/16) < 1.2 \text{ and } (x^2/9 + y^2/16) > 1 \\ 0.7 & \text{if } (x^2/9 + y^2/16) < 1 \text{ and } (x^2/9 + y^2/16) > 0.7 \\ 1.0 & \text{if } (x^2 + (y - 3.5)^2) < 0.25^2 \\ 0 & \text{others} \end{cases}.$$

Then, the simulated fan-beam raw data image (Fig. 9(a)) is generated by the forward algorithms of fan-beam described in Section 2.2. As shown in Figure 9(b), the reconstructed image, obtained by the reconstruction algorithm described in this article, exactly reveals the given attenuation coefficient function $f(x, y)$.

6. Conclusion

We have established a non-destructive testing software platform to generate parallel-beam or fan-beam raw data and to reconstruct the tomographic image of the scanned industrial components from raw data of 2D industrial CT. Except for the forward algorithms of parallel-beam and fan-beam, preprocess of original raw data, re-arrange algorithms and filtered back-projection (FBP) algorithms described in this article have been integrated into our software. Experimental results in Section 5 verified the efficiency and accuracy of our presented reconstruction algorithms including the preprocess algorithm. With these algorithms, the inner structure and subtle features of scanned objects have been clearly reconstructed from real fan-beam raw data and simulated raw data generated by our software. Furthermore, preprocess of raw data before reconstructions can efficiently eliminate the bad influence induced by mechanical devices of CT, which can greatly improve the reconstruction quality. Due to these advantages and the practicability of the presented reconstructed algorithms in this article, our software has been successfully applied in industrial non-destructive testing in CASC.

Acknowledgement

This work is supported by the National Science Fund for Distinguished Young Scholars of China under Grant No. 60225008, the Special Project of National Grand Fundamental Research 973 Program of China under Grant No. 2002CCA03900, the National Natural Science Foundation of China under Grant Nos. 90209008, 30370418, 60302016, 60172057, 30270403, Beijing Natural Science Fund under Grant No. 4042024.

References

[1] W.A. Kalender, K. Engelke and S. Schaller, Sprial CT: Medical use and potential industrial applications, *Proc. SPIE* **3149** (1997), 688–694.
[2] G.T. Herman, *Image Reconstruction from Projections: The Fundamentals of Computerized Tomography*, Academic Press, New York, 1980.
[3] A.C. Kak and M. Slaney, *Principles of Computerized Tomographic Imaging*, IEEE Press, New York, 1988.
[4] F. Natterer, *The Mathematics of Computerized Tomography*, John Wiley & Sons, New York, 1986
[5] B.K. Horn, Fan-beam reconstruction algorithms, *Proc. IEEE* **67** (1977), 1616–1623.

[6] P. Dreike and D.P. Boyd, Convolution reconstruction of fan-beam projections, *Comput. Graph. Image Process.* **5** (1976), 459–469.
[7] G.T. Gullberg, The reconstruction of fan-beam data by filtering the back-projection, *Comput. Graph. Image Process.* **10** (1979), 30–47.
[8] X. Pan, Optimal noise control in and fast reconstruction of fan-beam computed tomography image, *Med. Phys.* **26** (1999), 689–697.
[9] G. Besson, CT image reconstruction from fan-parallel data, *Med. Phys.* **26** (1999), 415–426.
[10] J. Hsieh, Reconstruction of X-ray helical computed tomography, *Med. Phys.* **23** (1996), 221–229.
[11] K. Taguchi and H.Aradate, Algorithm for image reconstruction in multi-slice helical CT, *Med. Phys.* **25** (1998), 550–560.
[12] Henrik Turbell, *Cone-beam reconstruction using filtered back-projection*, Ph.D. Dissertation, Linköping University, 2001.
[13] N. Frank, Numerical method in tomography, *Acta Numerica* **8** (1999), 107–141.